

# Mineral Detection of Cosmic-Ray Boosted Dark Matter

Jin-Wei Wang<sup>1,\*</sup> and Fei-Fei Li<sup>1</sup>

<sup>1</sup>*School of Physics, University of Electronic Science and Technology of China, Chengdu 611731, China*

We present the first dedicated analysis of cosmic-ray dark matter (CRDM) in paleo detectors. Owing to their large kinetic energies, CRDM particles generate nuclear-recoil tracks that extend to substantially larger lengths than those produced by dominant backgrounds from neutrinos and intrinsic radioactivity. Combined with the ultra-large effective geological exposure of  $\mathcal{O}(10^5)$  t yr, paleo detectors provide a uniquely sensitive probe of sub-GeV DM. Considering both constant and vector-mediator interactions, we find that paleo detectors improve the sensitivity to the DM–proton scattering cross section by one to two orders of magnitude compared with the latest XENONnT limits.

**Introduction.**—According to a broad range of astrophysical and cosmological observations, dark matter (DM) constitutes approximately 85% of the total matter content in the universe [1–6]. Despite its overwhelming abundance, the fundamental particle nature of DM remains unknown, rendering its identification one of the central challenges in contemporary particle physics. Under the assumption that DM interacts weakly with standard model (SM) particles, direct detection experiments provide a powerful and model-independent approach to probing its properties through nuclear and/or electron recoils. Leading experiments such as LUX-ZEPLIN (LZ) [7–9], XENONnT [10, 11], and PandaX-4T [12, 13] have achieved unprecedented sensitivities to weakly interacting massive particles (WIMPs) with masses in the GeV–TeV range. However, for sub-GeV and lighter DM, the sensitivity of conventional experiments rapidly deteriorates: halo DM in this mass regime carries insufficient kinetic energy to produce detectable recoils in detectors with typical thresholds at the  $\mathcal{O}(\text{keV})$  scale.

To overcome this limitation, several scenarios involving “boosted” DM populations have been proposed [14–20]. A particularly robust and unavoidable mechanism was identified in Ref. [18], where a small fraction of the Galactic DM halo is accelerated to relativistic energies through elastic scattering with high-energy cosmic rays (CRs). This component, commonly referred to as cosmic-ray boosted DM (CRDM), acquires sufficient kinetic energy to generate observable signals in terrestrial detectors, thereby enabling sensitivity to DM–nucleon interactions well below the GeV mass scale.

In this work, we demonstrate that ancient minerals—so-called paleo detectors—provide a uniquely powerful probe of CRDM. The detection principle of paleo detectors is straightforward: a DM particle scattering off a nucleus in a crystalline mineral produces a nuclear recoil, which subsequently traverses the lattice and deposits energy through ionization losses. In insulating materials, this process leaves permanent damage tracks that can be resolved with modern microscopy techniques at nanometer-scale spatial resolution. The resulting track length and morphology distributions thus provide a direct record of the underlying DM–nucleus interaction and

recoil kinematics.

Paleo detectors constitute a fundamentally different detection paradigm: rather than operating a detector in real time, one searches for the permanent damage tracks imprinted by nuclear recoils in natural minerals over geological timescales, up to  $\mathcal{O}(1)$  Gyr. A key advantage of paleo detectors lies in their enormous effective exposure. For example, 100 g of material that has been recording nuclear damage tracks for 1 Gyr yields an effective  $\mathcal{O}(10^5)$  t yr exposure, which is far beyond what is achievable in conventional experiments with  $\mathcal{O}(1)$  t yr exposure. This renders paleo detectors particularly well suited for probing extremely feeble interactions, such as DM [21–28] and neutrinos [27, 29–32].

Here, we present the first dedicated analysis of CRDM in paleo detectors. Owing to the large kinetic energies of CRDM particles, the resulting nuclear recoils produce track lengths that are significantly longer than the dominant short track backgrounds from neutrinos and intrinsic radioactivity. Consequently, paleo detectors can operate in a low-background regime, and in certain regions of parameter space, effectively background-free for CRDM searches. Combined with the ultra-large effective exposure of paleo detectors, we demonstrate that their sensitivities to the DM–proton scattering cross section surpass those of existing direct detection experiments by one to two orders of magnitude, depending on the underlying DM model. Our results establish paleo detectors as a powerful and complementary probe of sub-GeV DM and highlight their unique potential to explore regions of parameter space that are otherwise inaccessible to current and near-future experiments.

**CRDM flux.**— For the interaction between DM and nucleons, we consider two benchmark scenarios. The first is a phenomenological model with a constant DM–proton scattering cross section, denoted by  $\sigma_{\chi p}$ . The second is a simplified model with a massive vector mediator, described by the Lagrangian [33–35]

$$\begin{aligned} \mathcal{L} \supset & \bar{\chi} (i\gamma^\mu \partial_\mu - m_\chi) \chi + g_\chi \bar{\chi} \gamma^\mu \chi V_\mu \\ & + \sum_q g_q \bar{q} \gamma^\mu q V_\mu + \frac{1}{2} m_V^2 V_\mu V^\mu, \end{aligned} \quad (1)$$

where  $m_\chi$  and  $m_V$  denote the masses of the DM particle and the vector mediator, respectively, and  $g_\chi$  and  $g_q$  are the corresponding couplings to DM and quarks. Throughout this work we assume flavor-universal couplings between the mediator and quarks. Extensions to other interaction structures, such as scalar or axial-vector mediators, are straightforward and will not qualitatively alter our conclusions [36–39].

The local interstellar (LIS) population of CRs is well measured and is commonly characterized by their differential intensity  $dI/dR$  as a function of rigidity  $R$ . In this work, we adopt the LIS spectra from Ref. [40], where Galactic CR propagation and solar modulation are treated using **GALPROP** and **HELMOD**, respectively. These results are consistent with Voyager 1 observations [41] as well as AMS-02 measurements [42].

Cosmic-ray scattering on halo DM unavoidably produces a boosted DM component. The resulting differential CRDM flux can be written as

$$\frac{d\Phi_\chi}{dT_\chi} = D_{\text{eff}} \frac{\rho_\chi}{m_\chi} \sum_i \int_{T_i^{\text{min}}(T_\chi)}^{\infty} dT_i \frac{d\sigma_{\chi i}}{dT_\chi} \frac{d\Phi_i}{dT_i} \quad (2)$$

with

$$T_i^{\text{min}}(T_\chi) = \left( \frac{T_\chi}{2} - m_i \right) \left[ 1 \pm \sqrt{1 + \frac{2T_\chi}{m_\chi} \frac{(m_i + m_\chi)^2}{(2m_i - T_\chi)^2}} \right], \quad (3)$$

where the  $+$  ( $-$ ) sign applies for  $T_\chi > 2m_i$  ( $T_\chi < 2m_i$ ),  $\rho_\chi \simeq 0.3 \text{ GeV cm}^{-3}$  is the local DM density,  $T_\chi$  ( $T_i$ ) denotes the kinetic energy of DM (CR species  $i$ ), and  $d\sigma_{\chi i}/dT_\chi$  is the differential scattering cross section between DM and CR species  $i$ . The parameter  $D_{\text{eff}}$  represents the effective distance over which CR–DM scattering contributes to the local CRDM flux; throughout this work we take  $D_{\text{eff}} \simeq 9 \text{ kpc}$  [43]. We include the nine dominant CR species that account for more than 90% of the total CRDM flux, namely  $\{\text{H, He, C, N, O, Ne, Mg, Si, Fe}\}$  [43].

The differential scattering cross section  $d\sigma_{\chi i}/dT_\chi$  is model dependent. For the constant cross section scenario, we have

$$\frac{d\sigma_{\chi i}}{dT_\chi} = A_i^2 \frac{G_i^2(q^2)}{T_\chi^{\text{max}}(T_i)} \frac{\mu_{\chi i}^2}{\mu_{\chi p}^2} \sigma_{\chi p}, \quad (4)$$

with

$$T_\chi^{\text{max}}(T_i) = \frac{T_i^2 + 2m_i T_i}{T_i + (m_i + m_\chi)^2/(2m_\chi)}, \quad (5)$$

where  $A_i$  is the mass number of CR species  $i$ ,  $\mu_{\chi i}$  and  $\mu_{\chi p}$  are the reduced masses of the DM–nucleus and DM–proton systems, respectively, and  $G_i(q^2)$  denotes the nuclear form factor with momentum transfer  $q^2$ . For hydrogen and helium, we adopt the dipole form factor [18, 44], while for heavier nuclei we use the Helm form factor [35, 43, 45, 46].

For the vector-mediator scenario, both elastic and deep-inelastic scattering (DIS) processes contribute. The elastic DM–proton scattering cross section is given by [33–35]

$$\frac{d\sigma_{\chi i}^{\text{el}}}{dT_\chi} = 2m_\chi \frac{A_i^2 g_p^2 g_\chi^2}{4\pi\beta^2} \frac{G_p^2(Q^2)}{(Q^2 + m_V^2)^2} \left[ 1 - \frac{\beta^2 Q^2}{Q_{\text{max}}^2} + \frac{Q^4}{8m_\chi^2 E_i^2} \right], \quad (6)$$

where  $g_p = 3g_q$  is the effective DM–proton coupling,  $Q^2 \equiv -q^2$  is the positive four-momentum transfer squared,  $\beta = |\mathbf{p}_i|/E_i$  is the CR’s velocity. The maximal momentum transfer is

$$Q_{\text{max}}^2 = \frac{4(E_i^2 - m_i^2)m_\chi^2}{m_\chi^2 + m_i^2 + 2m_\chi E_i}. \quad (7)$$

At sufficiently high energies, inelastic scattering becomes important. We treat the DIS process using the standard Bjorken variables [47, 48], following Refs. [34, 35, 38, 49, 50]. The differential cross section is

$$\frac{d^2\sigma_{\chi p}^{\text{DIS}}}{dT_\chi d\mu_s} = \frac{m_\chi \sqrt{(T_p^2 + 2m_p T_p)(T_\chi^2 + 2m_\chi T_\chi)}}{m_p^2 E_\chi^2 y} \frac{d^2\sigma_{\text{DIS}}}{dxdy}, \quad (8)$$

where  $\mu_s$  is the cosine of the scattering angle, and  $x$  and  $y$  are the Bjorken variables. The partonic cross section reads

$$\begin{aligned} \frac{d^2\sigma_{\text{DIS}}}{dxdy} = & \frac{g_\chi^2 g_q^2}{4\pi(Q^2 + m_V^2)^2} \frac{2E_\chi^2 y}{E_\chi^2 - m_\chi^2} \\ & \times \left( 1 - y + \frac{y^2}{2} - \frac{xy m_p}{2E_\chi} - \frac{m_\chi^2}{2E_\chi m_p} \frac{y}{x} \right) F_2(x, Q^2), \end{aligned} \quad (9)$$

with the structure function

$$F_2(x, Q^2) = \sum_{f=u,d,c,s,b} [f(x, Q^2) + \bar{f}(x, Q^2)] x, \quad (10)$$

where  $f$  ( $\bar{f}$ ) are the parton distribution functions (PDFs) of quarks (antiquarks). We use the MSTW 2008 NNLO PDFs [51]. For scattering on CR nuclei, we approximate

$$\frac{d^2\sigma_{\chi i}^{\text{DIS}}}{dT_\chi d\mu_s} = R_i(x, Q^2) \left[ Z_i \frac{d^2\sigma_{\chi p}^{\text{DIS}}}{dT_\chi d\mu_s} + (A_i - Z_i) \frac{d^2\sigma_{\chi n}^{\text{DIS}}}{dT_\chi d\mu_s} \right], \quad (11)$$

where  $R_i(x, Q^2)$  denotes the nuclear modification factor, which is  $\mathcal{O}(1)$  [52, 53]. For simplicity, we set  $R_i(x, Q^2) \simeq 1$  in our numerical analysis. Integrating over the scattering angle, we obtain

$$\frac{d\sigma_{\chi i}^{\text{DIS}}}{dT_\chi} = \int d\mu_s \frac{d^2\sigma_{\chi i}^{\text{DIS}}}{dT_\chi d\mu_s}. \quad (12)$$

Combining Eqs. (2)–(12), we compute the CRDM flux for the different interaction scenarios. We focus on the

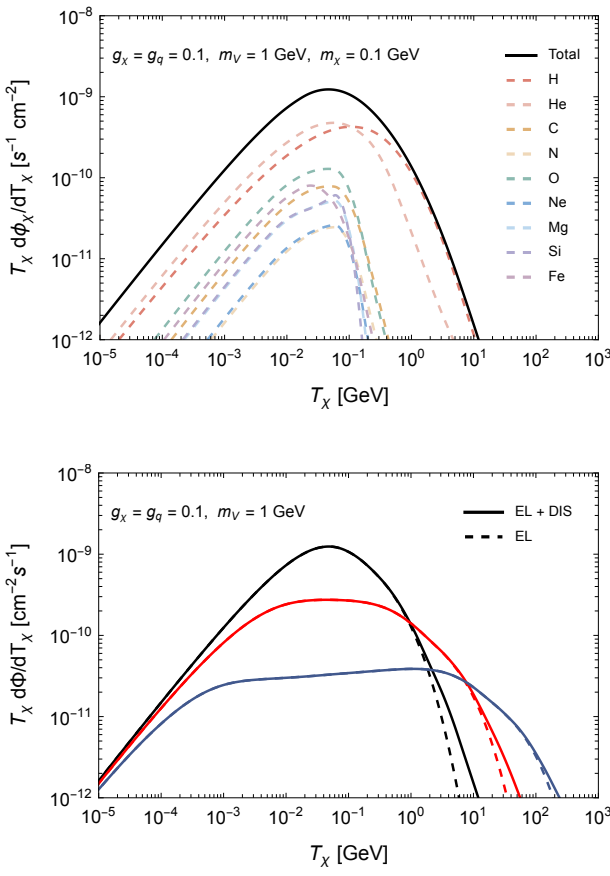


FIG. 1. Differential flux of CRDM for the vector-mediator model. (Top) Total CRDM spectrum (solid black) and the individual contributions from different cosmic-ray species (dashed), assuming  $g_\chi = g_q = 0.1$ ,  $m_V = 1$  GeV, and  $m_\chi = 0.1$  GeV. (Bottom) Impact of inelastic scattering on the CRDM flux: the solid curves include both elastic and deep-inelastic scattering (EL+DIS), while the dashed curves show the elastic-only contribution (EL). Different colours correspond to different DM mass  $m_\chi$ , namely  $m_\chi = 100$  MeV (black), 10 MeV (red), and 1 MeV (blue).

light DM regime,  $m_\chi \lesssim 0.1$  GeV, which is particularly well motivated for boosted DM searches. For the mediator mass we consider two benchmark values,  $m_V = 1$  GeV and  $m_V = 10$  MeV; results for other values of  $m_V$  can be inferred from these benchmarks.

In Fig. 1, we show the resulting CRDM spectra for the vector-mediator model. The upper panel displays the total CRDM flux (solid black), together with the individual contributions from different CR species (dashed). The lower panel illustrates the impact of inelastic scattering: the solid and dashed curves correspond to the full calculation (including both elastic and DIS processes) and to the elastic-only case, respectively. We consider three representative DM masses,  $m_\chi = 100$  MeV (black), 10 MeV (red), and 1 MeV (blue), and fix  $g_\chi = g_q = 0.1$  with  $m_V = 1$  GeV. As is evident from the figure, the

DIS contribution becomes increasingly important at high energies, demonstrating that inelastic processes must be included for an accurate description of the CRDM flux.

**CRDM track length spectrum.**— For both conventional direct detection experiments and paleo detectors, a key physical quantity is the CRDM-induced nuclear recoil rate on a target nucleus  $j$  with mass  $m_j$ . In direct detection experiments,  $j$  typically corresponds to xenon (Xe), whereas in paleo detectors it denotes the various constituent nuclei of the mineral. Since both techniques are sensitive only to relatively low nuclear recoil energies,  $T_j \lesssim \mathcal{O}(0.1)$  GeV, we restrict our analysis to elastic CRDM–nucleus scattering.

Using Eq. (2), the differential recoil rate is

$$\frac{d\Gamma_j}{dT_j} = \int_{T_\chi^{\min}(T_j)}^{\infty} dT_\chi \frac{d\sigma_{\chi j}}{dT_j} \frac{d\Phi_\chi}{dT_\chi}, \quad (13)$$

where  $d\sigma_{\chi j}/dT_j$  and the minimal CRDM energy  $T_\chi^{\min}(T_j)$  follow from Eqs. (6) and (3), with the replacements  $\chi \rightarrow j$  and  $i \rightarrow \chi$ .

The CRDM signal in paleo detectors is encoded in the spectrum of damage track lengths. The differential rate of tracks with reconstructed length  $x_T$  for an exposure  $\epsilon$  is given by [21–24]

$$\frac{dR}{dx_T} = \epsilon \sum_j \frac{\xi_j}{m_j} \frac{d\Gamma_j}{dT_j} \frac{dT_j}{dx_T}, \quad (14)$$

where  $\xi_j$  denotes the mass fraction of element  $j$  in the composite target, and  $dT_j/dx_T$  is the stopping power, evaluated using SRIM [54, 55]. Ions with charge  $Z \leq 2$  (in particular H and He) do not produce persistent tracks in most materials and are therefore neglected [22, 24].

Two complementary readout strategies have been proposed for paleo detectors [21–24]. The high-resolution scenario probes small samples (e.g.,  $\sim 10$  mg) with nanometer scale track length resolution, while the high-exposure scenario analyzes much larger samples (e.g.,  $\sim 100$  g) with coarser resolution (e.g.,  $\sim 15$  nm). In this work, we adopt the latter, which maximally exploits the large CRDM induced track lengths and the ultra large effective exposure.

The experimental observable is the binned track length spectrum. The expected number of events in the  $i$ -th bin,  $x_T \in [x_a, x_b]$ , is

$$N_i(x_a, x_b) = \int_0^{\infty} dx_T W(x_T; x_a, x_b) \frac{dR}{dx_T}, \quad (15)$$

with the window function

$$W(x_T; x_a, x_b) = \frac{1}{2} \left[ \text{erf} \left( \frac{x_T - x_a}{\sqrt{2}\sigma_{x_T}} \right) - \text{erf} \left( \frac{x_T - x_b}{\sqrt{2}\sigma_{x_T}} \right) \right], \quad (16)$$

which accounts for the finite readout resolution  $\sigma_{x_T}$ . We consider two representative minerals, Gypsum

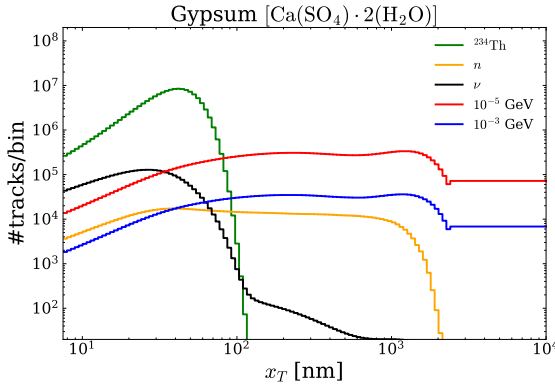


FIG. 2. Binned track length distributions in Gypsum  $[\text{Ca}(\text{SO}_4) \cdot 2(\text{H}_2\text{O})]$  for CRDM in the vector-mediator model. The red and blue curves show CRDM signals for  $m_\chi = 10^{-5}$  GeV and  $10^{-3}$  GeV, respectively, while the black, orange, and green curves denote the dominant nuclear recoil backgrounds from neutrinos, radiogenic neutrons, and  $^{238}\text{U} \rightarrow ^{234}\text{Th} + \alpha$  decays. The input parameters are  $g_\chi = g_q = 0.1$  and  $m_V = 1$  GeV.

$[\text{Ca}(\text{SO}_4) \cdot 2(\text{H}_2\text{O})]$  and Olivine  $[\text{Mg}_{1.6}\text{Fe}_{0.4}(\text{SiO}_4)]$ , and adopt a benchmark exposure of 100 g Gyr [21–28]. Other exposures can be obtained by simple rescaling.

Only nuclear recoils constitute relevant backgrounds for paleo detectors, since electron recoils do not leave stable tracks. The dominant background sources are neutrinos (solar, atmospheric, and supernova) [29, 56], radiogenic neutrons from the  $^{238}\text{U}$  decay chain, and recoils induced by  $^{234}\text{Th}$  [57, 58]. For the fiducial  $^{238}\text{U}$  concentrations, we adopt the same benchmark values as in Refs. [21–24], namely  $10^{-11}$  for Gypsum and  $10^{-10}$  for Olivine. Additional backgrounds, such as intrinsic crystal defects, are expected to be distinguishable from recoil tracks [29, 59]. Signal and background spectra are computed using `paleoSpec` [21, 22, 25, 29].

Fig. 2 shows the binned track length spectrum in Gypsum for the vector-mediator model with  $g_\chi = g_q = 0.1$  and  $m_V = 1$  GeV. The red and blue curves correspond to  $m_\chi = 10^{-5}$  GeV and  $10^{-3}$  GeV, respectively. A salient feature is the pronounced excess of CRDM-induced events at large track lengths, where all relevant backgrounds rapidly fall off. This long track regime, which is inaccessible to standard halo DM, provides an efficient and robust handle for background discrimination.

An additional important feature is the construction of the final, highest-track length bin. We choose the upper edge of this bin at  $x_T = 10 \mu\text{m}$  and set its lower boundary such that the expected number of neutron-induced background events is below 0.5. As a consequence, this bin effectively represents a background-free search region. The presence of CRDM-induced tracks extending into this regime therefore provides a powerful lever arm to

enhance the sensitivity of paleo detectors to boosted DM.

**Paleo detector constraints.**— For the vector-mediator scenario, to facilitate comparison with the literature, we define the DM–proton scattering cross section as

$$\sigma_{\chi p} = \frac{g_\chi^2 g_p^2}{\pi m_V^4} \mu_{\chi p}^2, \quad (17)$$

where  $\mu_{\chi p} = m_\chi m_p / (m_\chi + m_p)$  is the reduced mass. All experimental sensitivities are presented in the  $m_\chi$ – $\sigma_{\chi p}$  plane.

For paleo detectors, we follow the spectral likelihood approach of Ref. [24], which employs a profile likelihood ratio test statistic to derive projected sensitivities. Details of the statistical procedure can be found therein. Our numerical analysis is performed using the public code `paleoSens` [21, 22, 25, 29], which consistently incorporates detector response and background modeling.

For comparison, we also derive constraints from conventional direct detection using the latest XENONnT data with an exposure of  $\epsilon = 3.1 \text{ t yr}$  [60]. Applying a standard Poisson likelihood [61], we obtain a 90% C.L. upper limit on the number of CRDM-induced events,  $N_{\text{lim}} = 35.87$ .

The expected number of CRDM events in XENONnT is

$$N_{\text{CRDM}} = \frac{\epsilon}{m_{\text{Xe}}} \int_{T_{\text{exp}}^{\text{min}}}^{T_{\text{exp}}^{\text{max}}} dT_{\text{Xe}} \frac{d\Gamma_{\text{Xe}}}{dT_{\text{Xe}}}, \quad (18)$$

where  $[T_{\text{exp}}^{\text{min}}, T_{\text{exp}}^{\text{max}}] = [3.8, 64.1] \text{ keV}$  is energy range of sensitivity of XENONnT. The corresponding exclusion is obtained by imposing  $N_{\text{CRDM}} < N_{\text{lim}}$ .

Fig. 3 summarizes the resulting limits on  $\sigma_{\chi p}$ . The dotted curves correspond to the constant cross section scenario, while the dashed and solid curves denote the vector-mediator model with  $m_V = 10 \text{ MeV}$  and  $1 \text{ GeV}$ , respectively. The purple and green lines show the paleo detector sensitivities for Gypsum and Olivine, and the red curves indicate the XENONnT constraints. Existing limits from PandaX-4T [62], SENSEI [63], and BBN [64] are also shown for comparison.

As is evident, paleo detectors substantially outperform conventional direct detection experiments in the sub-GeV mass range, with sensitivities improved by one to two orders of magnitude, depending on the interaction model.

**Conclusion.**— We have presented the first dedicated study of CRDM in paleo detectors. We considered two benchmark DM–proton interaction scenarios, namely a constant cross section model and a vector-mediator model, and incorporated the dominant cosmic-ray contributions relevant for CRDM production.

Owing to the high kinetic energies of CRDM particles, the induced nuclear-recoil tracks extend to sub-

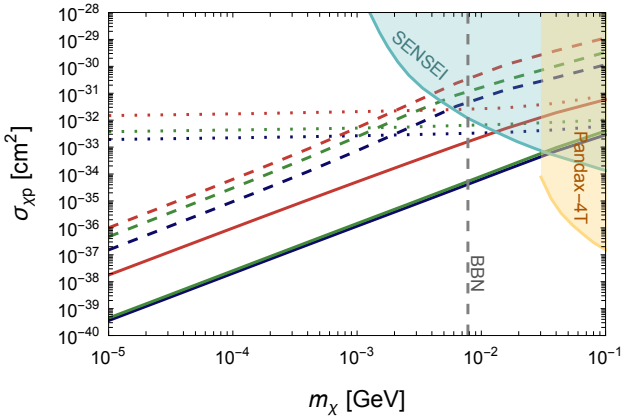


FIG. 3. Constraints on the DM–proton scattering cross section as a function of the DM mass. The purple and green curves show the projected sensitivities of paleo detectors using Gypsum and Olivine, respectively, while the red curves indicate the XENONnT limits. The dotted curves correspond to the constant cross section scenario, whereas the dashed and solid curves denote the vector-mediator model with  $m_V = 10$  MeV and  $m_V = 1$  GeV. Existing constraints from PandaX-4T [62], SENSEI [63], and BBN [64] are shown for comparison.

stantially larger lengths than those produced by dominant backgrounds from neutrinos and intrinsic radioactivity. As a result, paleo detectors can operate in an effectively background-free regime for CRDM searches. Together with their ultra-large effective geological exposure of  $\mathcal{O}(10^5)$  t yr, this enables sensitivities to the DM–proton scattering cross section that improve by up to two orders of magnitude compared with current direct detection limits, including those from XENONnT.

Our results establish paleo detectors as a powerful and complementary probe of boosted DM and motivate the use of geological materials as next generation DM detectors.

**Acknowledgments.**—The authors wish to thank Alessandro Granelli for the thoughtful discussions at the initial stage of this project. The work of J.-W.W. was supported by the National Natural Science Foundation of China (NSFC) under Grants No. 12405119, the Natural Science Foundation of Sichuan Province under Grant No. 2025ZNSFSC0880, and Fundamental Research Funds for the Central Universities (Grant No. Y030242063002070).

\* jinwei.wang@uestc.edu.cn

- [1] Gianfranco Bertone, Dan Hooper, and Joseph Silk, “Particle dark matter: Evidence, candidates and constraints,” *Phys. Rept.* **405**, 279–390 (2005), arXiv:hep-ph/0404175.
- [2] Marco Taoso, Gianfranco Bertone, and Antonio Masiero, “Dark Matter Candidates: A Ten-Point Test,” *JCAP* **03**, 022 (2008), arXiv:0711.4996 [astro-ph].
- [3] Gianfranco Bertone and Dan Hooper, “History of dark matter,” *Rev. Mod. Phys.* **90**, 045002 (2018), arXiv:1605.04909 [astro-ph.CO].
- [4] N. Aghanim *et al.* (Planck), “Planck 2018 results. VI. Cosmological parameters,” *Astron. Astrophys.* **641**, A6 (2020), [Erratum: *Astron. Astrophys.* 652, C4 (2021)], arXiv:1807.06209 [astro-ph.CO].
- [5] A. Arbey and F. Mahmoudi, “Dark matter and the early Universe: a review,” *Prog. Part. Nucl. Phys.* **119**, 103865 (2021), arXiv:2104.11488 [hep-ph].
- [6] Marco Cirelli, Alessandro Strumia, and Jure Zupan, “Dark Matter,” (2024), arXiv:2406.01705 [hep-ph].
- [7] D. S. Akerib *et al.* (LZ), “LUX-ZEPLIN (LZ) Conceptual Design Report,” (2015), arXiv:1509.02910 [physics.ins-det].
- [8] D. S. Akerib *et al.* (LZ), “Projected WIMP sensitivity of the LUX-ZEPLIN dark matter experiment,” *Phys. Rev. D* **101**, 052002 (2020), arXiv:1802.06039 [astro-ph.IM].
- [9] J. Aalbers *et al.* (LZ), “First Dark Matter Search Results from the LUX-ZEPLIN (LZ) Experiment,” *Phys. Rev. Lett.* **131**, 041002 (2023), arXiv:2207.03764 [hep-ex].
- [10] E. Aprile *et al.* (XENON), “Search for New Physics in Electronic Recoil Data from XENONnT,” *Phys. Rev. Lett.* **129**, 161805 (2022), arXiv:2207.11330 [hep-ex].
- [11] E. Aprile *et al.* (XENON), “First Dark Matter Search with Nuclear Recoils from the XENONnT Experiment,” *Phys. Rev. Lett.* **131**, 041003 (2023), arXiv:2303.14729 [hep-ex].
- [12] Hongguang Zhang *et al.* (PandaX), “Dark matter direct search sensitivity of the PandaX-4T experiment,” *Sci. China Phys. Mech. Astron.* **62**, 31011 (2019), arXiv:1806.02229 [physics.ins-det].
- [13] Yue Meng *et al.* (PandaX-4T), “Dark Matter Search Results from the PandaX-4T Commissioning Run,” *Phys. Rev. Lett.* **127**, 261802 (2021), arXiv:2107.13438 [hep-ex].
- [14] Kaustubh Agashe, Yanou Cui, Lina Necib, and Jesse Thaler, “(in)direct detection of boosted dark matter,” *J. Cosmol. Astropart. Phys.* **2014**, 062–062 (2014), arXiv:1405.7370.
- [15] Chris Kouvaris, “Probing light dark matter via evaporation from the Sun,” *Phys. Rev. D* **92**, 075001 (2015), arXiv:1506.04316.
- [16] Haipeng An, Maxim Pospelov, Josef Pradler, and Adam Ritz, “Directly Detecting MeV-Scale Dark Matter Via Solar Reflection,” *Phys. Rev. Lett.* **120**, 141801 (2018), arXiv:1708.03642.
- [17] Timon Emken, Chris Kouvaris, and Niklas Grønlund Nielsen, “The Sun as a sub-GeV dark matter accelerator,” *Phys. Rev. D* **97**, 063007 (2018), arXiv:1709.06573.
- [18] Torsten Bringmann and Maxim Pospelov, “Novel direct detection constraints on light dark matter,” *Phys. Rev. Lett.* **122**, 171801 (2019), arXiv:1810.10543 [hep-ph].
- [19] Jin-Wei Wang, Alessandro Granelli, and Piero Ul

lio, “Direct Detection Constraints on Blazar-Boosted Dark Matter,” *Phys. Rev. Lett.* **128**, 221104 (2022), arXiv:2111.13644 [astro-ph.HE].

[20] Alessandro Granelli, Piero Ullio, and Jin-Wei Wang, “Blazar-boosted dark matter at Super-Kamiokande,” *JCAP* **07**, 013 (2022), arXiv:2202.07598 [astro-ph.HE].

[21] Sebastian Baum, Andrzej K. Drukier, Katherine Freese, Maciej Górski, and Patrick Stengel, “Searching for Dark Matter with Paleo-Detectors,” *Physics Letters B* **803**, 135325 (2020), arXiv:1806.05991 [astro-ph.CO].

[22] Andrzej K. Drukier, Sebastian Baum, Katherine Freese, Maciej Górski, and Patrick Stengel, “Paleo-detectors: Searching for Dark Matter with Ancient Minerals,” *Physical Review D* **99**, 043014 (2019), arXiv:1811.06844 [astro-ph.CO].

[23] Thomas D. P. Edwards, Bradley J. Kavanagh, Christoph Weniger, Sebastian Baum, Andrzej K. Drukier, Katherine Freese, Maciej Górski, and Patrick Stengel, “Digging for dark matter: Spectral analysis and discovery potential of paleo-detectors,” *Physical Review D* **99**, 043541 (2019), arXiv:1811.10549 [hep-ph].

[24] Sebastian Baum, Thomas D. P. Edwards, Katherine Freese, and Patrick Stengel, “New Projections for Dark Matter Searches with Paleo-Detectors,” *Instruments* **5**, 21 (2021), arXiv:2106.06559 [astro-ph.CO].

[25] Sebastian Baum, William DeRocco, Thomas D. P. Edwards, and Saarik Kalia, “Galactic geology: Probing time-varying dark matter signals with paleodetectors,” *Physical Review D* **104**, 123015 (2021), arXiv:2107.02812 [astro-ph.GA].

[26] Joseph Bramante, Bradley J. Kavanagh, and Nirmal Raj, “Scattering Searches for Dark Matter in Subhalos: Neutron Stars, Cosmic Rays, and Old Rocks,” *Physical Review Letters* **128**, 231801 (2022), arXiv:2109.04582 [hep-ph].

[27] Sebastian Baum *et al.*, “Mineral detection of neutrinos and dark matter. A whitepaper,” *Phys. Dark Univ.* **41**, 101245 (2023), arXiv:2301.07118 [astro-ph.IM].

[28] Audrey Fung, Thalles Lucas, Levente Balogh, Matthew Leybourne, and Aaron C. Vincent, “Refining the sensitivity of new physics searches with ancient minerals,” *Phys. Rev. D* **112**, 043040 (2025), arXiv:2504.08885 [hep-ph].

[29] Sebastian Baum, Thomas D. P. Edwards, Bradley J. Kavanagh, Patrick Stengel, Andrzej K. Drukier, Katherine Freese, Maciej Górski, and Christoph Weniger, “Paleo-detectors for Galactic supernova neutrinos,” *Physical Review D* **101**, 103017 (2020), arXiv:1906.05800 [astro-ph.GA].

[30] Johnathon R. Jordan, Sebastian Baum, Patrick Stengel, Alfredo Ferrari, Maria Cristina Morone, Paola Sala, and Joshua Spitz, “Measuring Changes in the Atmospheric Neutrino Rate Over Gigayear Timescales,” *Phys. Rev. Lett.* **125**, 231802 (2020), arXiv:2004.08394 [hep-ph].

[31] Natalia Tapia-Arellano and Shunsaku Horiuchi, “Measuring solar neutrinos over gigayear timescales with paleo detectors,” *Phys. Rev. D* **103**, 123016 (2021), arXiv:2102.01755 [hep-ph].

[32] Sebastian Baum, Francesco Capozzi, and Shunsaku Horiuchi, “Rocks, water, and noble liquids: Unfolding the flavor contents of supernova neutrinos,” *Phys. Rev. D* **106**, 123008 (2022), arXiv:2203.12696 [hep-ph].

[33] Gang Guo, Yue-Lin Sming Tsai, Meng-Ru Wu, and Qiang Yuan, “Elastic and Inelastic Scattering of Cosmic Rays on Sub-GeV Dark Matter,” *Phys. Rev. D* **102**, 103004 (2020), arXiv:2008.12137 [astro-ph.HE].

[34] Liangliang Su, Lei Wu, and Bin Zhu, “An improved bound on accelerated light dark matter,” *Sci. China Phys. Mech. Astron.* **67**, 221012 (2024), arXiv:2308.02204 [hep-ph].

[35] Jin-Wei Wang, “Blazar-boosted dark matter: Novel signatures via elastic and inelastic scattering,” *Phys. Rev. D* **112**, 055004 (2025), arXiv:2503.22105 [hep-ph].

[36] Andrea Giovanni De Marchi, Alessandro Granelli, Jacopo Nava, and Filippo Sala, “Did IceCube discover Dark Matter around Blazars?” (2024), arXiv:2412.07861 [astro-ph.HE].

[37] Liangliang Su, Lei Wu, Ning Zhou, and Bin Zhu, “Accelerated-light-dark-matter-Earth inelastic scattering in direct detection,” *Phys. Rev. D* **108**, 035004 (2023), arXiv:2212.02286 [hep-ph].

[38] Andrea Giovanni De Marchi, Alessandro Granelli, Jacopo Nava, and Filippo Sala, “Boosted dark matter versus dark matter-induced neutrinos from single and stacked blazars,” *JHEP* **12**, 136 (2025), arXiv:2507.12278 [hep-ph].

[39] Andrea Giovanni De Marchi, Alessandro Granelli, Jacopo Nava, and Filippo Sala, “Diffuse astrophysical neutrinos from dark matter around blazars,” *Phys. Lett. B* **871**, 140015 (2025), arXiv:2506.06416 [hep-ph].

[40] M. J. Boschini *et al.*, “Inference of the Local Interstellar Spectra of Cosmic-Ray Nuclei  $Z \leq 28$  with the Gal-Prop–HelMod Framework,” *Astrophys. J. Suppl.* **250**, 27 (2020), arXiv:2006.01337 [astro-ph.HE].

[41] A. C. Cummings, E. C. Stone, B. C. Heikkila, N. Lal, W. R. Webber, G. Jóhannesson, I. V. Moskalenko, E. Orlando, and T. A. Porter, “Galactic Cosmic Rays in the Local Interstellar Medium: Voyager 1 Observations and Model Results,” *Astrophys. J.* **831**, 18 (2016).

[42] M. Aguilar *et al.* (AMS), “Properties of Neon, Magnesium, and Silicon Primary Cosmic Rays Results from the Alpha Magnetic Spectrometer,” *Phys. Rev. Lett.* **124**, 211102 (2020).

[43] Chen Xia, Yan-Hao Xu, and Yu-Feng Zhou, “Production and attenuation of cosmic-ray boosted dark matter,” *JCAP* **02**, 028 (2022), arXiv:2111.05559 [hep-ph].

[44] I. Angeli, “A consistent set of nuclear rms charge radii: properties of the radius surface  $R(N,Z)$ ,” *Atom. Data Nucl. Data Tabl.* **87**, 185–206 (2004).

[45] Richard H. Helm, “Inelastic and elastic scattering of 187-mev electrons from selected even-even nuclei,” *Phys. Rev.* **104**, 1466–1475 (1956).

[46] J. D. Lewin and P. F. Smith, “Review of mathematics, numerical factors, and corrections for dark matter experiments based on elastic nuclear recoil,” *Astropart. Phys.* **6**, 87–112 (1996).

[47] Andy Buckley, James Ferrando, Stephen Lloyd, Karl Nordström, Ben Page, Martin Rüfenacht, Marek Schönherr, and Graeme Watt, “LHAPDF6: parton density access in the LHC precision era,” *Eur. Phys. J. C* **75**, 132 (2015), arXiv:1412.7420 [hep-ph].

[48] Rabah Abdul Khalek, Rhorry Gauld, Tommaso Giani, Emanuele R. Nocera, Tanjona R. Rabemananjara, and Juan Rojo, “nNNPDF3.0: evidence for a modified partonic structure in heavy nuclei,” *Eur. Phys. J. C* **82**, 507 (2022), arXiv:2201.12363 [hep-ph].

[49] S. Navas *et al.* (Particle Data Group), “Review of particle physics,” *Phys. Rev. D* **110**, 030001 (2024).

[50] Joshua Berger, “A Module for Boosted Dark Matter Event Generation in GENIE,” (2018), [arXiv:1812.05616 \[hep-ph\]](https://arxiv.org/abs/1812.05616).

[51] A. D. Martin, W. J. Stirling, R. S. Thorne, and G. Watt, “Parton distributions for the LHC,” *Eur. Phys. J. C* **63**, 189–285 (2009), [arXiv:0901.0002 \[hep-ph\]](https://arxiv.org/abs/0901.0002).

[52] K. Kovarik *et al.*, “nCTEQ15 - Global analysis of nuclear parton distributions with uncertainties in the CTEQ framework,” *Phys. Rev. D* **93**, 085037 (2016), [arXiv:1509.00792 \[hep-ph\]](https://arxiv.org/abs/1509.00792).

[53] Kari J. Eskola, Petja Paakkinen, Hannu Paukkunen, and Carlos A. Salgado, “EPPS16: Nuclear parton distributions with LHC data,” *Eur. Phys. J. C* **77**, 163 (2017), [arXiv:1612.05741 \[hep-ph\]](https://arxiv.org/abs/1612.05741).

[54] J. P. Biersack and J. F. Ziegler, “The stopping and range of ions in solids,” in *Ion Implantation Techniques*, edited by Heiner Ryssel and Hans Glawischnig (Springer Berlin Heidelberg, Berlin, Heidelberg, 1982) pp. 122–156.

[55] James F. Ziegler, M. D. Ziegler, and J. P. Biersack, “SRIM – The stopping and range of ions in matter (2010),” *Nucl. Instrum. Meth. B* **268**, 1818–1823 (2010).

[56] Ciaran A. J. O’Hare, “Can we overcome the neutrino floor at high masses?” *Phys. Rev. D* **102**, 063024 (2020), [arXiv:2002.07499 \[astro-ph.CO\]](https://arxiv.org/abs/2002.07499).

[57] Juan I. Collar, “Comments on ‘limits on dark matter using ancient mica’,” *Phys. Rev. Lett.* **76**, 331 (1996), [arXiv:astro-ph/9511055](https://arxiv.org/abs/astro-ph/9511055).

[58] D. P. Snowden-Ifft, E. S. Freeman, and P. B. Price, “Snowden-Ifft, Freeman, and Price Reply (A Reply to the Comment by Juan I Collar),” *Phys. Rev. Lett.* **76**, 332 (1996).

[59] S. Demouchy, “Defects in olivine,” *European Journal of Mineralogy* **33**, 249–282 (2021).

[60] E. Aprile *et al.* (XENON), “WIMP Dark Matter Search Using a 3.1 Tonne-Year Exposure of the XENONnT Experiment,” *Phys. Rev. Lett.* **135**, 221003 (2025), [arXiv:2502.18005 \[hep-ex\]](https://arxiv.org/abs/2502.18005).

[61] P. A. Zyla *et al.* (Particle Data Group), “Review of Particle Physics,” *PTEP* **2020**, 083C01 (2020).

[62] Di Huang *et al.* (PandaX), “Search for Dark-Matter–Nucleon Interactions with a Dark Mediator in PandaX-4T,” *Phys. Rev. Lett.* **131**, 191002 (2023), [arXiv:2308.01540 \[hep-ex\]](https://arxiv.org/abs/2308.01540).

[63] Prakruth Adari *et al.* (SENSEI), “First Direct-Detection Results on Sub-GeV Dark Matter Using the SENSEI Detector at SNOLAB,” *Phys. Rev. Lett.* **134**, 011804 (2025), [arXiv:2312.13342 \[astro-ph.CO\]](https://arxiv.org/abs/2312.13342).

[64] Cara Giovanetti, Mariangela Lisanti, Hongwan Liu, and Joshua T. Ruderman, “Joint Cosmic Microwave Background and Big Bang Nucleosynthesis Constraints on Light Dark Sectors with Dark Radiation,” *Phys. Rev. Lett.* **129**, 021302 (2022), [arXiv:2109.03246 \[hep-ph\]](https://arxiv.org/abs/2109.03246).